

# Constraining the SMEFT with a differential cross section measurement of $tWZ$ production at the HL-LHC.

---

James Keaveney<sup>a,1</sup>

<sup>a</sup> *University of Cape Town,  
University Avenue, Cape Town, South Africa*

*E-mail:* [james.keaveney@uct.ac.za](mailto:james.keaveney@uct.ac.za)

ABSTRACT: A prospective measurement of the differential cross section of  $tWZ$  production with respect to the transverse momentum of the  $Z$  boson using a general-purpose detector at the High-Luminosity Large Hadron Collider (HL-LHC) is described. Constraints on the Standard Model Effective Field Theory (SMEFT) enabled by the measurement are estimated. Uncertainties and inter-bin correlations are used to determine the measurement's expected covariance matrix. A parametric model of the differential cross section in the SMEFT is constructed and, together with the expected covariance matrix, is used to determine the expected posterior probability function of six SMEFT Wilson coefficients. Expected 95% Bayesian credible intervals for each coefficient and pair of coefficients are derived by marginalising this posterior function. The intervals suggest that the measurement will result in a constraint on the  $c_{tZ}$  coefficient that is tighter than that obtained from existing analyses. For the other coefficients, the measurement will likely provide weaker constraints than those derived from other HL-LHC measurements involving top quarks and  $Z$  bosons. However, as the measurement is simultaneously sensitive to many coefficients, it will provide a useful input to a SMEFT analysis that considers multiple operators.

---

<sup>1</sup>Corresponding author.

---

## Contents

<b>1</b>	<b>Introduction</b>	<b>1</b>
<b>2</b>	<b>The <math>tWZ</math> process at the HL-LHC</b>	<b>1</b>
<b>3</b>	<b>Differential cross sections in the SMEFT</b>	<b>3</b>
<b>4</b>	<b>Constraining SMEFT coefficients</b>	<b>5</b>
<b>5</b>	<b>Conclusion and outlook</b>	<b>8</b>

---

## 1 Introduction

The relevance of the top quark’s couplings to theories of new physics are well documented [1–4]. Given the lack of evidence of resonant production of new particles in the Large Hadron Collider (LHC) data, attention has turned to new physics scenarios in which new particles have masses around an energy scale  $\Lambda$  that is large with respect to the scales directly probed at the LHC. The Standard Model Effective Field Theory (SMEFT) is a theoretical framework that describes the effects of such heavy new particles on lower energy observables. The SMEFT Lagrangian is obtained by extending the SM Lagrangian with higher-order operators. In the work presented here, only the dominant, dimension-6 operators are considered with the contribution of each operator to the Lagrangian scaled by a dimensionless Wilson coefficient  $c_i$  divided by  $\Lambda^2$ . If the scale of new physics is indeed large with respect to the LHC energies, significant deviations of measurements of  $c_i$  from the SM expectation ( $c_i = 0$ ) may be the first evidence of new physics. As the particle physics community prepares for the HL-LHC where proton collision datasets of unprecedented size will be produced, it is crucial to identify previously unexplored measurements that have the potential to improve the precision at which  $c_i$  can be determined. In this document, the potential of a measurement of one such observable, the differential cross section of  $tWZ$  production, at a general-purpose detector is explored.

## 2 The $tWZ$ process at the HL-LHC

The  $tWZ$  process refers to the electroweak production of a single top quark in association with a  $W$  boson and a  $Z$  boson. In 13 TeV proton collisions,  $tWZ$  is predicted to have a SM cross section of  $\approx 160$  fb at NLO in QCD [6]. The modelling of this process at NLO in QCD has been explored in [6] and the sensitivity of the inclusive  $tWZ$  cross section to the SMEFT coefficients has been quantified in [7, 8]. As the  $Z$  boson may be radiated from the initial-state bottom quark, the final-state top quark, or the final-state  $W$  boson, the process already exhibits complex phenomenology at LO in the SM by simultaneously

embedding the  $t$ - $Z$ ,  $b$ - $Z$ , and  $W$ - $Z$  electroweak couplings. Consequently, the  $tWZ$  process is sensitive to multiple SMEFT operators. These operators modify SM interaction vertices and generate new vertices not present in the SM. Not all of the operators that affect the  $tWZ$  process involve the top quark field. Although the primary goal of this work is to estimate potential constraints on SMEFT coefficients related to top quark couplings, ignoring all other operators that affect the  $tWZ$  process could lead to an overestimation of the precision of the constraints. Therefore the following set of six operators are chosen on the basis of them having a significant effect on either the overall rate or kinematics of the  $tWZ$  process. However the list is not exhaustive and investigation of the expected complex interplay within a larger set of operators in an NLO cross section calculation is left to future work. Similarly, interference effects at NLO between the  $tWZ$  and  $t\bar{t}Z$  processes will be important to a future analysis of  $tWZ$  measurements at the HL-LHC in the SMEFT. In this paper, the implementation of the SMEFT in the SMEFTATNLO package [10] is adopted. The operator definitions in SMEFTATNLO follow the Warsaw basis outlined in [11]. In this convention the chosen operators are namely:  $\mathcal{O}_{tZ}$ ,  $\mathcal{O}_{tW}$ ,  $\mathcal{O}_{\phi t}$ ,  $\mathcal{O}_{\phi q}^{(3)}$ ,  $\mathcal{O}_{\phi q}^{(M)} = \mathcal{O}_{\phi q}^{(1)} - \mathcal{O}_{\phi q}^{(3)}$ , and  $\mathcal{O}_{tG}$ . The advantages of  $tWZ$  measurements in constraining the SMEFT coefficients are detailed in [8]. The effect of the SMEFT operators on the  $tWZ$  process show an energy dependence that is more pronounced than that of alternative processes such as  $tZq$ . Thus as more data is recorded and measurements of higher-energy phase space of  $tWZ$  become possible, constraints on SMEFT coefficients from  $tWZ$  will continue to improve after constraints from processes with weaker energy dependence become saturated. This serves as particular motivation to assess the potential of measuring  $\frac{d\sigma_{tWZ}}{dp_T}$  as a probe of the high-energy phase space of  $tWZ$ .

In order to estimate the constraints on the SMEFT coefficients obtainable with a measurement of  $\frac{d\sigma_{tWZ}}{dp_T}$  at the HL-LHC, estimates of the expected experimental uncertainties and inter-bin covariances in the measurement are crucial. Due to large backgrounds, it is likely that only the decay channels where the  $Z$  boson decays to a pair of oppositely-charged electrons or muons and at least one other electron or muon is present will yield useful precision. Assuming a total integrated luminosity of  $3000 \text{ fb}^{-1}$ , and an event selection efficiency of 40 % introduced by event selection criteria, the total number of  $tWZ$  events ( $N_{tWZ}$ ) usable for the measurement of  $\frac{d\sigma_{tWZ}}{dp_T}$  is estimated as:

$$N_{tWZ} = \sigma_{tWZ} \times BR \times \mathcal{L} \times \epsilon = 116 \times 0.026 \times 3000 \times 0.4 \approx 5000$$

The statistical uncertainties within each bin depend on the chosen binning scheme. Increasing the number of bins will yield greater sensitivity to the SMEFT coefficients as the shape of the distributions is measured in greater detail. Furthermore the number of coefficients that can be independently constrained by a single absolute differential cross section is limited by the number of bins. Conversely, statistical uncertainties in each bin increase as the number of bins increases, degrading the constraints on the SMEFT coefficients. A binning scheme that consisting of five equal-width bins between 0 and 500 GeV that aims to balance these concerns is adopted. The expectation for the differential cross section from the SM is estimated by a fixed-order calculation at LO performed by MAD-

GRAPH5\_AMC@NLO. The statistical uncertainty in a given bin is estimated as the square root of the number of events expected assuming the NLO inclusive cross section, branching ratio, efficiency, and luminosity described above. A relative systematic uncertainty of 7% is assumed in each bin based on comparable differential cross section measurements by the CMS experiment using 13 TeV LHC data [21]. In Figure 1, the expected central values of the  $\frac{d\sigma_{tWZ}}{dp_T}$  measurement along with statistical and systematic uncertainties are shown. Differential cross sections are typically measured after an unfolding procedure in which the resolution effects of the detector response are accounted for. The unfolding procedure introduces statistical correlations between the measured values of  $\frac{d\sigma_{tWZ}}{dp_T}$  in the bins of the unfolded differential cross section due to migrations of events across bin boundaries. Similarly, sources of systematic uncertainty that cause correlated effects in multiple bins introduce additional inter-bin correlations. An existing measurement of the differential cross section of  $t\bar{t}$  production in the dilepton channel as a function of the  $p_T$  of the dilepton system,  $\frac{d\sigma_{t\bar{t}}}{dp_T}$ , using 13 TeV proton collision data the CMS experiment [21] is used to approximate the correlation matrix of the expected data from the measurement of  $\frac{d\sigma_{tWZ}}{dp_T}$  at the HL-LHC. The central values, uncertainties, and the full covariance matrix of the CMS measurement is available at [22, 23]. The CMS measurement is of the  $t\bar{t}$  process and is performed in the experimental conditions of the CMS experiment at the LHC. These factors will result in different uncertainties and thus covariances to those of the measurement of  $\frac{d\sigma_{tWZ}}{dp_T}$  at the HL-LHC. Inter-bin correlations depend mainly on detector resolutions and experimental and theoretical uncertainties and are likely to be reduced at the HL-LHC. The covariances of the HL-LHC measurement are thus conservatively estimated by combining its uncertainties with the correlation matrix of the CMS measurement. The correlation matrix of the CMS data is estimated by taking the outer product of a vector of the binned total uncertainties of the CMS data with itself and performing an element-wise division of the covariance matrix of the CMS data by this outer product. The last two bins of the CMS measurement are disregarded in order to produce a correlation matrix with numbers of rows and columns equal to the number of bins in the  $\frac{d\sigma_{tWZ}}{dp_T}$  measurement. The covariance matrix of the  $\frac{d\sigma_{tWZ}}{dp_T}$  measurement is estimated by a element-wise multiplication of the correlation matrix derived from the CMS data with the outer product of a vector of expected total uncertainties of the  $\frac{d\sigma_{tWZ}}{dp_T}$  measurement with itself. This covariance matrix is used to estimate constraints on the SMEFT coefficients presented in section 4.

### 3 Differential cross sections in the SMEFT

If the SMEFT Lagrangian contains  $n$  dimension-6 operators  $c_i$  and the number of such operators in each Feynman diagram is limited to one, any cross section in the SMEFT can be expressed as a  $2^{nd}$  order multivariate polynomial in  $c_i$ :

$$\sigma(c_i) = \sigma_{SM} + \sum_{i=1}^{i=n} \frac{c_i}{\Lambda^2} \beta_i + \sum_{j=1}^{j=n} \sum_{i=1}^{i=n} \frac{c_i c_j}{\Lambda^4} \beta_{ij}$$

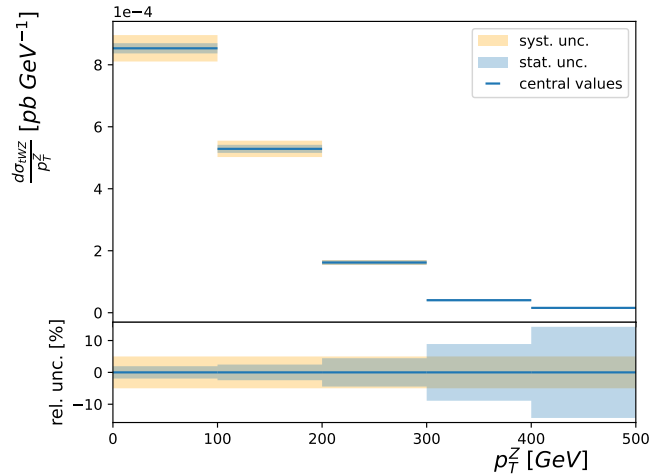


**Figure 1.** The expected central values of  $\frac{d\sigma_{tWZ}}{dp_T^Z}$  in bins of  $p_T^Z$  along with expected statistical and systematic are shown in the upper panel. The lower panel shows the statistical and systematic uncertainties expressed as percentages of the central values.

In this expression,  $\sigma(c_i)$  is the cross section in the SMEFT, written explicitly as a function of the  $n$  SMEFT coefficients and  $\sigma_{SM}$  is the SM cross section. The  $\frac{c_i}{\Lambda^2}\beta_i$  terms represent the contributions from the product of the SM amplitude and the amplitudes of diagrams containing a dimension-6 vertex. The group of terms  $\frac{c_i c_j}{\Lambda^4}\beta_{ij}$  represent the  $n^2$  contributions from the products of amplitudes of diagrams containing a vertex from the  $i^{th}$  operator with the amplitudes of diagrams containing a vertex from the  $j^{th}$  operator and thus includes the contributions from the squares of the amplitudes of diagrams containing a vertex from the  $i^{th}$  operator. As  $\frac{c_i c_j}{\Lambda^4}\beta_{ij} = \frac{c_j c_i}{\Lambda^4}\beta_{ji}$ , only  $\binom{n}{2}$  independent contributions are present in the  $\sum_{j=1}^{j=n} \sum_{i=1}^{i=n} \frac{c_i c_j}{\Lambda^4}\beta_{ij}$  term. The terms  $\sigma_{SM}$ ,  $\beta_{i,1}$  and  $\beta_{i,j}$ , are specific to the process and represent the  $b$  unknowns of the polynomial where  $b = 1 + n + \binom{n}{2}$ . Thus for  $n$  operators,  $b$  is the  $(n+1)^{th}$  triangular number. If the  $\sigma$  and  $\beta$  terms are vectors with elements corresponding to the contributions to the differential cross section within each bin, then the polynomial represents a parametric model of a differential cross section. An exact solution for the unknowns of the polynomial can be found by making a minimum number of theoretical calculations for  $\sigma_{SMEFT}$  at distinct points in  $c_i$  space and forming a system of linear equations in an approach known as *morphing* [17]. An alternative approach based on Bayesian reasoning is presented in [18]. In general, Monte-Carlo based theoretical predictions carry significant statistical uncertainties, especially in regions of phase space with small cross sections. Furthermore, in SMEFT calculations involving multiple operators, one or more of the unknowns may be extremely small relative to the others at all of the points in  $c_i$  space used to construct the system of linear equations. Hence these relatively small unknowns can be imprecisely determined by the exact solution to the linear system. When contributions associated to these unknowns become large in other regions of the SMEFT coefficient space, inaccuracies in the predictions of the morphing model can arise.

The approach pursued here, termed *regression morphing*, alleviates this issue. Instead of producing an exact solution of a system of linear equations, the unknowns are determined by minimising the sum of squared differences  $S$  between  $p$  theoretical predictions for the differential cross section at randomly distributed points in the SMEFT coefficient space and the corresponding predictions of the regression morphing model. For a model derived from  $p$  predictions, each with  $q$  bins,  $S$  is defined as

$$S(\vec{\beta}) = \sum_{i=1}^{i=p} \sum_{j=1}^{j=q} (d\sigma_{i,j} - x(\vec{\beta})_{i,j})^2$$

where  $S$  is written explicitly as a function of a vector of the model's unknowns  $\vec{\beta}$ ,  $d\sigma_{i,j}$  is the differential cross section in the  $j^{\text{th}}$  bin of the  $i^{\text{th}}$  theoretical prediction and  $x(\vec{\beta})_{i,j}$  is the corresponding prediction of the model. The regression morphing model can be made arbitrarily accurate in any region of the SMEFT coefficient space by including a sufficient number of predictions when minimising  $S$ .

#### 4 Constraining SMEFT coefficients

To construct a regression morphing model for  $\frac{d\sigma_{tWZ}}{dp_T^Z}$  at the HL-LHC, 150 *training* predictions for  $\frac{d\sigma_{tWZ}}{dp_T^Z}$  13 TeV proton collisions were generated at random points in the  $c_i$  space. The predictions were produced with the SMEFTATNLO [10] package implemented in the MADGRAPH5\_AMC@NLO Monte Carlo generator version v2\_6\_7 [16] at LO in QCD and in fixed-order mode. Although fixed-order predictions lack the parton shower and hadronisation modelling usually important to the modelling of hadron collider observables, the speed of generation and lack of a need to process large MC event samples makes them invaluable in the construction of regression morphing models and are sufficient to demonstrate the sensitivity of  $\frac{d\sigma_{tWZ}}{dp_T^Z}$  to the SMEFT coefficients. Similarly, the usage of NLO predictions would yield more precise estimates of  $\frac{d\sigma_{tWZ}}{dp_T^Z}$  and expected constraints on the  $c_i$ . However, NLO predictions would require either the application of a diagram removal scheme to suppress components of the  $tWZ$  calculation that overlap with the  $t\bar{t}Z$  process or a calculation that fully accounts for overlapping components and associated interference effects. Such a theoretical treatment is left to future work. To validate the model, 30 *test* predictions, statistically independent from the training predictions, were generated at random points in the SMEFT coefficient space and compared to the corresponding predictions of the model. The binned residuals between the test predictions and model predictions expressed as percentages of the test predictions are Gaussian-distributed with a mean of -0.0005 % and standard deviation of 0.0089 %, demonstrating that the inaccuracies in the model are negligible. The posterior probability density function  $p(c_i|x, \Sigma)$  is used to derive constraints on the six SMEFT coefficients where  $c_i$  are the SMEFT coefficients,  $x$  are expected measured values of  $\frac{d\sigma_{tWZ}}{dp_T^Z}$  in the SM scenario, and  $\Sigma$  is the estimated covariance matrix of  $x$  given the previously stated assumptions on uncertainties and correlations. The expected data are assumed to be Gaussian-distributed hence the log-likelihood is approximated as a  $\chi^2$  function accounting for the inter-bin correlations of the data introduced by

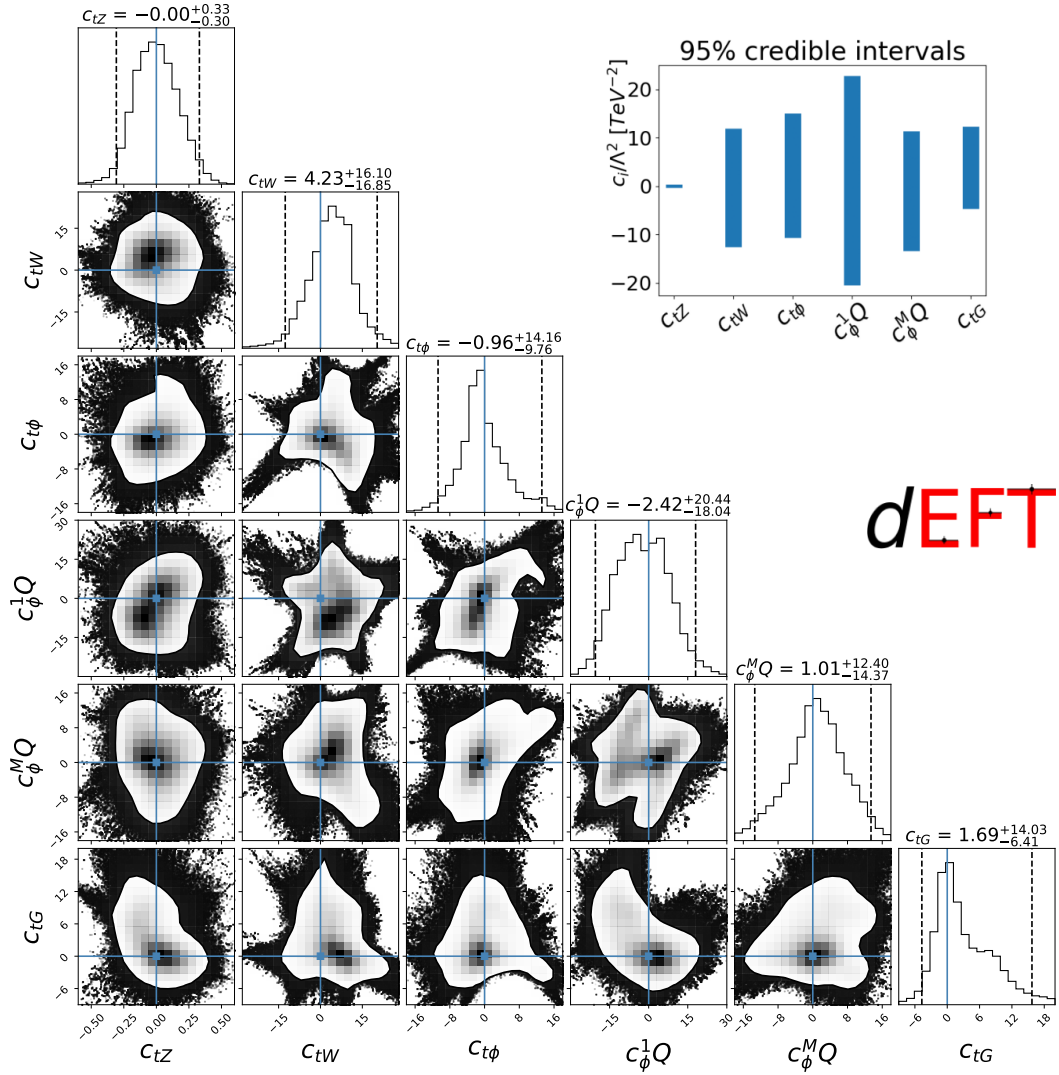


**Figure 2.** An array of the marginalised posterior probability density functions is shown. The 1-D functions for each of the SMEFT coefficients are placed along the grid diagonal. For each 1-D function, the vertical dashed lines bound the 95% credible interval. The 2-D functions for each pair of coefficients are shown in the other grid spaces. The white regions on the 2-D functions are CIs constructed to coincide with the 1-D CIs.

the *unfolding* process used to correct for detector resolution effects. This leads to the final expression for  $p(c_i|x, \Sigma)$ :

$$p(c_i|x, \Sigma) = p(c_i)(-0.5)(d(c_i, x)^T \Sigma^{-1} d(c_i, x))$$

where  $p(c_i)$  is the prior probability of the SMEFT coefficients,  $d(\frac{c_i}{\Lambda^2}, x)$  is a column vector of the residuals between the regression morphing model and expected data for the coefficient values  $\frac{c_i}{\Lambda^2}$ ,  $d(\frac{c_i}{\Lambda^2}, x)^T$  is the transpose of  $d(\frac{c_i}{\Lambda^2}, x)$ , and  $\Sigma^{-1}$  is the inverse of the covariance matrix of the expected data. This expression ignores the constant factor present in the canonical definition of the posterior probability which has no effect on the constraints. The



prior probability is chosen to be constant as a function of all SMEFT coefficients within an allowed region that is much larger than the expected 95% credible intervals (CI) of the posterior function and zero elsewhere. The central values of the expected data are chosen to match the prediction of the model in the SM ( $c_i = 0$ ) hypothesis. A numerical estimation of  $p(c_i|x, \Sigma)$  is produced using the `emcee` package [13] that implements a Markov Chain Monte Carlo algorithm. The constraint on a given single SMEFT coefficient is defined as the 95% CI of the 1-D pdf obtained by marginalising  $p(c_i|x, \Sigma)$  over the other coefficients centered around 0. In Figure 2, the 1- and 2-D marginalised posterior functions are shown in a grid arrangement. The marginalisations of  $p(c_i|x, \Sigma)$  are performed with the `corner` package [12]. The median values of the posterior function and the positive and negative distances to the edges of the CI are shown in text above each 1-D pdf. The edges of 95% CI centered around the median for each of the six 1-D functions are illustrated by vertical dashed lines. The blue lines indicate the SM expectation ( $c_i$ ). The white regions on the 2-D distributions are CIs constructed as to coincide with the 1-D CIs. The SM expectations for the  $c_i$  are indicated by intersections of the blue lines. An additional plot with the final constraints is provided in the upper-right corner of the figure. The construction and validation of the regression morphing model as well as interfaces to `emcee` and `corner` is provided by `dEFT`, a python package available on GitHub<sup>1</sup>. The sensitivity of  $\frac{d\sigma_{tWZ}}{dp_T^Z}$  to all six coefficients is apparent by the finite widths of the CI. Positive and negative correlations between the values of  $c_\phi^1 Q$  and  $c_\phi^M Q$  and  $c_{t\phi}$  and  $c_{tW}$  are apparent in the shape of the corresponding 2-D functions. These correlations could be mitigated by utilising an alternative differential distribution or by including measurements of other processes such as  $t\bar{t}Z$  and  $tZq$  that are sensitive to subsets of these operators. In Figure 3, the constraints are shown alongside frequentist 95% confidence intervals on subsets of these six coefficients reported a set of four other analyses for the purposes of broad comparison. The set comprises an analysis of an array of top quark measurements using LHC data with the SMEFiT framework [20], constraints from a measurement of the differential cross section at 13 TeV from the CMS experiment [15], expected constraints from a measurement of the inclusive  $t\bar{t}Z$  cross section at the HL-LHC by the CMS experiment [14] and an estimation of the constraints obtainable from a future measurement of the  $t\bar{t}Z$  cross section at the HL-LHC in the channel where the  $Z$  boson decays to a pair of neutrinos [5]. Due to the LO modelling of the  $tWZ$  signal, the approximations made to derive expected uncertainties and covariances of the  $\frac{d\sigma_{tWZ}}{dp_T^Z}$  measurement, and the different statistical definitions of the constraints, quantitative comparison of the constraints is difficult. However it is apparent that the constraint on  $c_{tZ}$  derived from the measurement of  $\frac{d\sigma_{tWZ}}{dp_T^Z}$  will be stronger than those already obtained from LHC data using the SMEFiT framework [20] and differential measurements of  $t\bar{t}Z$  production from CMS and similar to those expected by the CMS experiment in a HL-LHC scenario [14] and those expected in [5]. While the constraints on the other  $c_i$  appear significantly weaker than those from other measurements, the large number of operators affecting  $\frac{d\sigma_{tWZ}}{dp_T^Z}$  suggests that this observable will be useful in improving

<sup>1</sup>The `dEFT` codebase is available under a GNU GENERAL PUBLIC LICENSE at [dEFT on GitHub](#).



constraints in analysis simultaneously utilising large sets of top quark measurements.

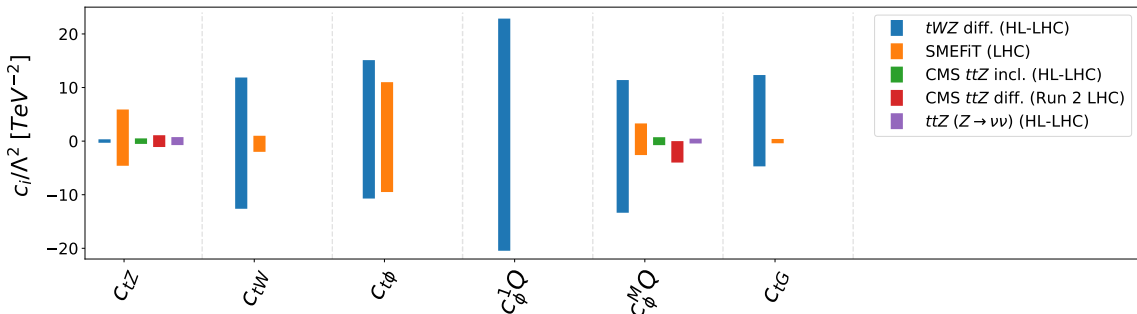


**Figure 3.** The expected 1-D 95% CI on the six SMEFT coefficients produced in this work are shown by the blue bars. Frequentist 95% confidence intervals on subsets of these coefficients reported elsewhere are shown for broad comparison [5, 14, 15, 20].

## 5 Conclusion and outlook

An analysis of the effects of a set of six dimension-6 operators in the SMEFT on the differential cross section of  $tWZ$  production with respect to the transverse momentum of the  $Z$  boson is presented. Estimates of the uncertainties and covariances of the a measurement based on LHC data are used to estimate the expected constraints on the SMEFT coefficients. A method termed regression morphing is used to construct a parametric model of  $\frac{d\sigma_{tWZ}}{dp_T}$  as a function of the SMEFT coefficients. A numerical approximation of the expected posterior probability function is derived. Constraints on the coefficients are defined as 95% credible intervals determined by marginalising the posterior probability function. In the case of  $c_{tZ}$ , the expected constraint is stronger than one derived from an array of LHC measurements and is comparable to expected constraints from measurements of the inclusive  $t\bar{t}Z$  cross section at the HL-LHC and the differential  $t\bar{t}Z$  cross section at the LHC. The measurement will also constrain the other coefficients to a lesser degree than other HL-LHC measurements and LHC measurements considered. Hence we conclude that measurements of  $\frac{d\sigma_{tWZ}}{dp_T}$  at the HL-LHC will be an important input to a global analysis of SMEFT coefficients with the potential to increase the discovery potential for new physics in the top quark sector in the HL-LHC data.

## Acknowledgments

The author would like to acknowledge the usage of the High Performance Computing cluster at the University of Cape Town and to thank Ilaria Brivio and Stephen Farry for much useful feedback.

## References

- [1] H. Georgi, L. Kaplan, D. Morin and A. Schenk, *Phys. Rev. D* **51** (1995), 3888-3894 doi:10.1103/PhysRevD.51.3888 [arXiv:hep-ph/9410307 [hep-ph]].
- [2] F. Bezrukov and M. Shaposhnikov, *J. Exp. Theor. Phys.* **120** (2015), 335-343 doi:10.1134/S1063776115030152 [arXiv:1411.1923 [hep-ph]].
- [3] M. Beneke, I. Efthymiopoulos, M. L. Mangano, J. Womersley, A. Ahmadov, G. Azuelos, U. Baur, A. Belyaev, E. L. Berger and W. Bernreuther, et al. [arXiv:hep-ph/0003033 [hep-ph]].
- [4] T. M. P. Tait and C. P. Yuan, *Phys. Rev. D* **63** (2000), 014018 doi:10.1103/PhysRevD.63.014018 [arXiv:hep-ph/0007298 [hep-ph]].
- [5] D. Haji Raissi, J. Ebadi and M. Mohammadi Najafabadi, *Phys. Rev. D* **101** (2020) no.9, 095002 doi:10.1103/PhysRevD.101.095002 [arXiv:2004.07615 [hep-ph]].
- [6] O. Bessidskaia Bylund [ATLAS], [arXiv:1612.00440 [hep-ph]].
- [7] F. Maltoni, L. Mantani and K. Mimasu, *JHEP* **10** (2019), 004 doi:10.1007/JHEP10(2019)004 [arXiv:1904.05637 [hep-ph]].
- [8] K. Mimasu, [arXiv:2105.10261 [hep-ph]].
- [9] Samuel van Beek et al, *Constraining the SMEFT with Bayesian reweighting*, *SciPost Phys.* **7** (2019).
- [10] C. Degrande, G. Durieux, F. Maltoni, K. Mimasu, E. Vryonidou and C. Zhang, [arXiv:2008.11743 [hep-ph]].
- [11] B. Grzadkowski, M. Iskrzynski, M. Misiak and J. Rosiek, *JHEP* **10** (2010), 085 doi:10.1007/JHEP10(2010)085 [arXiv:1008.4884 [hep-ph]].
- [12] Foreman-Mackey, Daniel. *Journal of Open Source Software* 1.2 (2016): 24. 10.21105/joss.00024
- [13] Foreman-Mackey, Daniel et al. *Publications of the Astronomical Society of the Pacific* 125.925 (2013): 306–312. [arXiv:1202.3665 [astro-ph.IM]].
- [14] CMS Collaboration CMS-PAS-FTR-18-036 <https://cds.cern.ch/record/2652018>
- [15] A. M. Sirunyan *et al.* [CMS], *JHEP* **03** (2020), 056 doi:10.1007/JHEP03(2020)056 [arXiv:1907.11270 [hep-ex]].
- [16] R. Frederix, S. Frixione, V. Hirschi, D. Pagani, H. S. Shao and M. Zaro, *JHEP* **07** (2018), 185 doi:10.1007/JHEP07(2018)185 [arXiv:1804.10017 [hep-ph]].
- [17] The ATLAS collaboration (2015). ATL-PHYS-PUB-2015-047.
- [18] N. Castro, J. Erdmann, C. Grunwald, K. Kröninger and N. A. Rosien, *Eur. Phys. J. C* **76** (2016) no.8, 432 doi:10.1140/epjc/s10052-016-4280-9 [arXiv:1605.05585 [hep-ex]].
- [19] M. Baak, S. Gadatsch, R. Harrington and W. Verkerke, *Nucl. Instrum. Meth. A* **771** (2015), 39-48 doi:10.1016/j.nima.2014.10.033 [arXiv:1410.7388 [physics.data-an]].
- [20] N. P. Hartland, F. Maltoni, E. R. Nocera, J. Rojo, E. Slade, E. Vryonidou and C. Zhang, *JHEP* **04** (2019), 100 doi:10.1007/JHEP04(2019)100 [arXiv:1901.05965 [hep-ph]].
- [21] The CMS collaboration (2019). *JHEP* 02 (2019) 149. [https://doi.org/10.1007/JHEP02\(2019\)149](https://doi.org/10.1007/JHEP02(2019)149)

- [22] The CMS collaboration (2019). <https://doi.org/10.17182/hepdata.89307>
- [23] The CMS collaboration (2019). <https://doi.org/10.17182/hepdata.89307.v1/t146>